Development of optimal models of porous media by combining static and dynamic data: The permeability and porosity distributions

Hossein Hamzehpour,[1] M. Reza Rasaei,[2] and Muhammad Sahimi[3,*]
[1]*Institute for Advanced Studies in Basic Sciences, Gava Zang, Zanjan 45195-1159, Iran*
[2]*Institute for Petroleum Engineering, University of Tehran, Tehran 11365-4563, Iran*
[3]*Mork Family Department of Chemical Engineering & Materials Science, University of Southern California, Los Angeles, California 90089-1211, USA*

(Received 19 November 2006; revised manuscript received 18 February 2007; published 22 May 2007)

We describe a method for the development of the optimal spatial distributions of the porosity ϕ and permeability k of a large-scale porous medium. The optimal distributions are constrained by static and dynamic data. The static data that we utilize are limited data for ϕ and k, which the method honors in the optimal model and utilizes their correlation functions in the optimization process. The dynamic data include the first-arrival (FA) times, at a number of receivers, of seismic waves that have propagated in the porous medium, and the time-dependent production rates of a fluid that flows in the medium. The method combines the simulated-annealing method with a simulator that solves numerically the three-dimensional (3D) acoustic wave equation and computes the FA times, and a second simulator that solves the 3D governing equation for the fluid's pressure as a function of time. To our knowledge, this is the first time that an optimization method has been developed to determine *simultaneously* the global minima of *two* distinct total energy functions. As a stringent test of the method's accuracy, we solve for flow of two immiscible fluids in the same porous medium, *without* using any data for the two-phase flow problem in the optimization process. We show that the optimal model, in addition to honoring the data, also yields accurate spatial distributions of ϕ and k, as well as providing accurate quantitative predictions for the single- and two-phase flow problems. The efficiency of the computations is discussed in detail.

DOI: 10.1103/PhysRevE.75.056311 PACS number(s): 47.56.+r, 91.60.Np, 05.40.−a

I. INTRODUCTION

In a previous paper [1], hereafter referred to as Part I, we described a new method for computing the optimal spatial distribution of the porosity ϕ of *large-scale* (LS) porous media—those that are much larger than laboratory-scale porous formations. Examples of such porous media include oil, gas, and geothermal reservoirs, and groundwater aquifers. Such porous media are very heterogeneous, with the heterogeneities manifesting themselves [2–4] as broad and correlated spatial distributions of the porosity and permeability, and the anisotropy caused by stratification (layering) of the porous formations. The presence of fractures and faults makes such porous media even more heterogeneous [2,4]. The development of accurate models for such porous media has been the subject of numerous studies over the past several decades [2–4].

The method proposed in Part I is one of optimization, whereby a certain amount of data for a given porous formation is utilized and the simulated-annealing (SA) [5] technique (or any other efficient optimization method) is used in order to compute the optimal porosity distribution that, in addition to honoring (preserving) the data, also satisfies the constraints that the data impose on the problem. In the past, a broad class of techniques, usually referred to as *reconstruction*, was proposed [6–9] for developing models of *laboratory-scale* porous materials. Such techniques use a limited amount of experimental data for some properties of the porous materials, which typically represent one-point (volume fraction) and two-point correlation functions. A variant of the SA technique was proposed by Torquato and co-workers [10], which can, in principle, be used with any type and number of correlation functions.

In the present paper, we extend the method proposed in Part I to the *simultaneous* optimization of the spatial distributions of the porosity ϕ *and* permeability k of a LS porous medium, which may then be used in the simulation of multiphase fluid flow and transport in that medium. As explained below, not only is the extension nontrivial, but also entails additional extensive numerical simulations. As pointed out in Part I, experimental data that are usually available for LS porous media may be divided into two important groups.

(i) *Direct* data, which include those for the two most important properties of LS porous media, namely, their porosity and permeability k which can be estimated by *in situ* nuclear-magnetic resonance [11], or by coring and laboratory measurements. Assuming that the morphology of a porous medium is not altered significantly over the period of time of practical interest in the medium, both ϕ and k represent *static* data.

(ii) *Indirect* data, the most important of which, in addition to the data for history-dependent pressure or production rates, are those that result from propagation of seismic waves in a porous medium. Seismic data provide estimates of the porosity distribution, as well as insight into the spatial distributions of the fractures, faults, and strata. Both the seismic records and time-dependent pressures or production rates of a fluid flowing through a LS porous medium represent *dynamic* data.

*Electronic address: moe@iran.usc.edu

In this paper we utilize both types of data and the SA method in order to develop the optimal spatial distributions of ϕ and k. We assume, (a) that limited data are available for ϕ and k, measured along certain directions (for example, along some wells), and (b) that we also have some data for the first-arrival (FA) times of seismic waves that reach a number of receivers installed in the porous medium, and for the time-dependent flux of a fluid which is flowing through the porous medium. The waves are produced by a source at a point, or a line or a plane of such point sources. The advantage of the FA times data is that they are usually available in large amounts. Likewise, extensive data for time-dependent pressures or fluxes of a fluid flowing through a porous medium are routinely recorded.

In order to compute the FA times in the course of optimization, we solve the three-dimensional (3D) wave equation. The most important advantage of doing so is that it is not subject to the high-frequency assumption that is essential to the traditional methods [12] in which the FA times are estimated by ray tracing. To utilize the data for the time-dependent pressures or fluxes of a fluid that flows through the porous medium, we solve numerically the 3D governing flow equation.

To further test the optimal porosity and permeability distributions, we carry out numerical simulation of flow of two immiscible fluids, such as water and oil, in the porous medium. Such simulation represents the most stringent test of the accuracy of the optimal porosity and permeability distributions. The reason is that flow of two immiscible fluids in a disordered porous medium is a percolation process [2,4,13] and, therefore, is highly sensitive to the spatial distribution of the connectivity of the low- and high-permeable zones. We use no data about the two-phase flow in the optimization process. Therefore if the optimal distributions of ϕ and k can provide accurate predictions for the displacement of one fluid by another immiscible fluid, they can be viewed as accurate and reliable.

The rest of this paper is as follows. The problem that we study is defined precisely in Sec. II. Section III presents the details of the numerical simulation of the equations that describe the propagation of seismic waves, and of the flow of a single fluid, in a porous medium. Section IV describes the formulation of the problem in terms of the objective (energy) functions of an optimization process, while Sec. V presents the details of the optimization algorithm based on the SA method. Section VI describes how the two-phase flow problem in the model porous medium is solved after the optimal model is developed. The results are presented in Sec. VII. We describe in Sec. VIII the conditions under which the method converges to the true solution of the problem, while the efficiency of the computations and their scaling with the size of the computational grid is discussed in Sec. IX. The paper is summarized in Sec. X.

II. PROBLEM STATEMENT

The model for the porous medium is the same as in Part I, namely, it is a computational grid of size $L_x \times L_y \times L_z$, and consists of cubic grid blocks to which the effective values of ϕ and k, as well as the bulk modulus $K(\phi)$, are assigned. In the present work we used $L_x=L_y=L_z=15$. Larger grids can also be simulated at higher computational cost but, for the purpose of illustrating the method, the size that we use suffices. In Sec. IX we discuss the method's computational cost and the simulations with larger grids.

Consistent with typical LS porous media (for example, oil reservoirs), we assume that there are a number of wells in the porous medium along which ϕ has been measured, and for which some data for k are also available. In the present work we assume that there are five wells in the z (vertical) direction, positioned at grid blocks $(3,3,n)$, $(3,L_z-2,n)$, $(L_z-2,3,n)$, $[(L_z+1)/2,(L_z+1)/2,n]$, and (L_z-2,L_z-2,n), with, $n=1,\ldots,L_z$. The effective porosities of such blocks are assumed to be known and are fixed during the optimization process. We also assume that the permeabilities of the same blocks are known, either measured directly, or (as sometimes done in practice) have been estimated through an empirical relationship between ϕ and k.

It is also assumed that the first-arrival (FA) times—the times at which the wave front first reaches certain points—have been recorded by a number of receivers that are distributed throughout the porous medium. Three different wave sources are used: (a) point source at the grid's center; (b) line source at the grid's center in the vertical direction (along one of the wells); and (c) a planar source on the grid's top plane. The receivers are on the five wells, except when the line source is along one of the wells, in which case the receivers are placed on the other four wells.

In addition, we assume that some data for the time-dependence of the rate of production of a single fluid from a location in the porous medium are available. The fluid is injected into the grid block with its center at (1, 1, 1), and produced at (L_x,L_y,L_z). Such information, which is known [2,4,14] as the *pressure-transient* (PT) data, is routinely collected in practical applications involving, for example, oil reservoirs. The question is, what are the optimal spatial distributions of ϕ and k that honor (preserve) their known values, and reproduce as closely as possible the data for the seismic waves FA times and the PT data?

III. NUMERICAL SIMULATION OF THE GOVERNING EQUATIONS

In this section, we describe the numerical simulation of propagation of seismic waves in, and flow of a single fluid through, a heterogeneous porous medium.

A. Numerical simulation of seismic wave propagation

Propagation of seismic waves in a porous medium is assumed to be described by the 3D acoustic wave equation, given by [15]

$$\rho(\mathbf{x})\frac{\partial^2}{\partial t^2}\psi(\mathbf{x},t) - \nabla \cdot [K(\mathbf{x})\,\nabla\,\psi(\mathbf{x},t)] = S(\mathbf{x},t), \qquad (1)$$

where $\psi(\mathbf{x},t)$ is the wave amplitude at time t, $K(\mathbf{x})$ and $\rho(\mathbf{x})$ are, respectively, the bulk modulus and density of the solid porous medium, and $S(\mathbf{x},t)$ is the source function for the

waves. Clearly, $\rho=\rho_0(1-\phi)$, where ρ_0 is the density of the pure solid mineral phase of rock. In Part I we considered a dry porous medium, since we were interested only in the optimal distribution of ϕ. In the present paper we study wet porous media, as we include fluid flow data in the optimization process. For this purpose, the Gassmann relation [16,17],

$$\frac{K}{K_0-K}=\frac{K_{\mathrm{dry}}}{K_0-K_{\mathrm{dry}}}+\frac{K_f}{\phi(K_0-K_f)}, \tag{2}$$

used heavily in the past, is utilized. Here, K_f and K_{dry} are, respectively, the bulk moduli of the fluid saturating the porous medium and that of the dry rock, while K_0 is the bulk modulus of the pure solid mineral phase. Among numerous empirical, semiempirical, and approximate theoretical relations that have been suggested in the past [18,19] for $K_{\mathrm{dry}}(\phi)$, we use

$$K_{\mathrm{dry}}=K_0(1-\phi)^{3/(1-\phi)}, \tag{3}$$

first suggested by Krief *et al.* [20].

To solve Eq. (1), we use the fully explicit finite-difference (FD) method with a second-order discretization for the time derivative,

$$\frac{\partial^2\psi(\mathbf{x},t)}{\partial t^2}\simeq\frac{\psi_{i,j,k}^{(n+1)}-2\psi_{i,j,k}^{(n)}+\psi_{i,j,k}^{(n-1)}}{\Delta t^2}+O(\Delta t^2), \tag{4}$$

where Δt is the time step's size, $\psi_{i,j,k}^{(n)}$ denotes the wave's amplitude at (discrete) time n, and $\mathbf{x}=(i,j,k)$ represents the center of a grid block. As for the spatial derivatives, we use the fourth-order FD approximation. Thus, for example,

$$\frac{\partial^2\psi(\mathbf{x},t)}{\partial x^2}\simeq\frac{-\psi_{i+2,j,k}^{(n)}+16\psi_{i+1,j,k}^{(n)}-30\psi_{i,j,k}^{(n)}+16\psi_{i-1,j,k}^{(n)}-\psi_{i-2,j,k}^{(n)}}{12\Delta x^2}, \tag{5}$$

where Δx is the grid blocks' size in the x direction.

When the source for the seismic waves is at the computational grid's center, or is represented by a line (of individual point sources) along the well at the grid's center in the vertical direction, reflective boundary conditions are used. Most natural porous media are stratified (anisotropic), and in a practical application of propagation of seismic waves in a porous formation (for, e.g., exploration) the main direction z of wave propagation may more or less be *perpendicular* to the planes of the strata, as the waves' source is typically on the ground surface. Thus we also consider the case in which the source is on the top xy plane that represents the ground surface, and use periodic boundary conditions in the horizontal xy planes, while the main wave front propagates in the z (vertical) direction. We used the following source function to generate the waves:

$$S(\mathbf{x}_s,t)=-A\exp[-\zeta(t-t_0)^2], \tag{6}$$

where A is a constant, ζ controls the wavelength of the wave, and $\mathbf{x}_s$ is the source's location. The wave equation, discretized by the fully explicit FD method, is then solved numerically, by starting from the grid blocks around the source, computing the waves' amplitude there, and then marching on to their neighbors until the wave has reached the entire computational grid. The FA times for all the grid points are then computed. The (dimensionless) time step is $\Delta t=10^{-3}$. The FA times for the receivers are utilized as the "data," while the rest are set aside for later comparison with the FA times that are computed using the optimal ϕ distribution.

All the receivers are placed along the wells (which is typically what is done in practice). When a point source is used for generating the seismic waves, the number of receivers is 74, the total number of grid blocks along the five wells (except for the one representing the source). With a line source, the number of receivers is 60—the number of grid blocks along four of the wells (the blocks along the fifth well at the grid's center represent the waves' source). Finally, with a planar source at the top the number of receivers is 70, placed along the five wells, except on the top (xy) plane.

B. Simulation of single-phase flow

The continuity equation for the flowing fluid is given by

$$\frac{\partial(\phi\rho_f)}{\partial t}+\nabla\cdot(\rho_f\mathbf{v})=G, \tag{7}$$

where $\mathbf{v}$ and ρ_f are, respectively, the fluid's velocity and density, and G represents a source (at the injection point) or sink (at the production point). We assume that the flow of the fluid is slow enough that the Darcy's law, $\mathbf{v}=-(k/\mu)\nabla P$, is applicable, where P is the pressure, and μ the fluid's viscosity. Furthermore, for a slightly compressible fluid, $\rho_f=\rho_{f0}+c\rho_{f0}(P-P_0)$, where c is the compressibility factor, P_0 is a constant reference pressure, and $\rho_{f0}=\rho_f(P=P_0)$. Thus the continuity equation (7) is turned into the governing equation for the fluid's pressure P:

$$\frac{1}{\mu c}\nabla\cdot(k\nabla P)+\frac{1}{\rho_f c}G=\phi\frac{\partial P}{\partial t}. \tag{8}$$

The source-sink term G is usually written as

$$G_i=I_{wi}(P_i-P)>0 \quad \text{source},$$

$$G_o=I_{wo}(P_o-P)<0 \quad \text{sink}, \tag{9}$$

where P_i and P_o are usually referred to as the *bottom-hole pressures*, while I_{wi} and I_{wo} are two constants called the *well indices* [3,4,14]. Equations (9) are necessitated by the fact that the grid blocks' linear size, and in particular that of those that are intersected by an injection or production well, is much larger than the well's physical radius. Therefore one must either have a highly resolved grid structure around the wells (which is not practical), or treat the injection-production sites through such equations as Eqs. (9).

To solve Eq. (8), we discretize it using the fully implicit FD method. At each time step, the resulting set of linear equations is solved using the biconjugate-gradient method. No-flow boundaries are imposed, and the initial condition is assumed to be $P(t=0)=0$. The (dimensionless) time step is $\Delta t=10^{-3}$.

IV. THE OBJECTIVE FUNCTIONS AND WEIGHT FACTORS

Since we search for the optimal distributions of ϕ and k, we must define two corresponding objective (energy) functions, E_ϕ and E_k, that are minimized by the SA method. Based on the ϕ and k data, we construct the corresponding correlation functions that are then utilized in E_ϕ and E_k. Then,

$$E_\phi = W_{Q_\phi} E_{Q_\phi} + W_w E_w + W_{C_\phi} E_{C_\phi}, \tag{10}$$

$$E_k = W_{Q_k} E_{Q_k} + W_{C_k} E_{C_k}. \tag{11}$$

Here,

$$E_{Q_\phi} = \sum_{t=1}^{t_{\max}} |Q_\phi^{(m)}(t) - Q_\phi^{(s)}(t)| \tag{12}$$

is the contribution to E_ϕ of the dynamic data in terms of the production flow rates, with $t_{\max}$ being the maximum time at which the production flow rates have been recorded. $Q_\phi^{(m)} \times(t)$ is the measured production flow rate at time t, while $Q_\phi^{(s)}(t)$ is the corresponding rate computed from the numerical simulation of Eq. (8). Likewise,

$$E_{Q_k} = \sum_{t=1}^{t_{\max}} |Q_k^{(m)}(t) - Q_k^{(s)}(t)| \tag{13}$$

is the contribution to E_k of the dynamic data in terms of the production flow rates. Moreover,

$$E_w = \sum_{i=1}^{N_r} |t_m(i) - t_s(i)| \tag{14}$$

is the contribution to E_ϕ of the seismic data in terms of the FA times, with N_r being the number of receivers at which the FA times have been recorded. Here, $t_m(i)$ is the measured FA time at receiver i, and $t_s(i)$ the corresponding value computed by the numerical simulation of Eq. (1). Finally, E_{C_ϕ} and E_{C_k} are the contributions to E_ϕ and E_k due to the correlation functions of the ϕ and k data. We have considered several types of distributions of ϕ and k that we describe shortly.

W_{Q_ϕ}, W_w, and W_{C_ϕ} are, respectively, the weight factors for the contributions to the total energy by the production flow rates, the FA times, and the correlation properties of the ϕ data. Such weight factors are, in general, different and attribute the proper importance to each component of E_ϕ. They are estimated before the optimization process begins. Each of them is inversely proportional to the average change of its corresponding energy function [21],

$$W_{Q_\phi} \propto (\langle |\Delta E_{Q_\phi}| \rangle)^{-1}, \tag{15}$$

$$W_w \propto (\langle |\Delta E_w| \rangle)^{-1}, \quad W_{C_\phi} \propto (\langle |\Delta E_{C_\phi}| \rangle)^{-1},$$

and, likewise, for the weight factors W_{Q_k} and W_{C_k},

$$W_{Q_k} \propto (\langle |\Delta E_{Q_k}| \rangle)^{-1}, \quad W_{C_k} \propto (\langle |\Delta E_{C_k}| \rangle)^{-1}. \tag{16}$$

It remains to specify the correlations functions of the ϕ and k distributions, so that the energy functions E_{C_k} and E_{C_ϕ} can also be specified. While any correlation function can be used, we note that analysis of the data for the spatial distribution of ϕ and k for many LS porous media indicates [2–4,14] that they contain long-range correlations. Such correlations may be described by a fractional Brownian motion (FBM), or other self-affine distributions. Recent works [22,23] indicate that, in addition to fluid flow and transport processes [2–4,14], such long-range correlations have important implications for wave propagation in LS porous media as well. Thus we assume that both the ϕ and k data along the wells follow the statistics of the FBM. The two-point correlation function $C(r)$ of a FBM is given by

$$C(r) = C_1 r^{2H}, \tag{17}$$

where $C_1 = C(r=1)$, and H is the Hurst exponent that characterizes the type of the correlations, such that for $H > 1/2$ ($H < 1/2$) one has persistent or positive (antipersistent or negative) correlations in the successive increments of the FBM, while for $H = 1/2$ the trace of an FBM follows Brownian motion. Another important property of a FBM is that its successive increments follow a Gaussian distribution (albeit with long-range correlations). Due to stratification, however, natural porous media are almost always anisotropic. If the strata are more or less in the xy planes, with z representing the vertical direction perpendicular to them, one must define two correlation functions,

$$C_{xy}(r) = C_1^{(xy)} r^{2H}, \quad C_z(r) = C_1^{(z)} r^{2H}. \tag{18}$$

In this case, E_C, the contribution of the correlation function of ϕ (k) is written as $E_C \simeq E_C^{(xy,r)} + E_C^{(z,r)}$, with

$$E_C^{(xy,r)} = \sum_{k=1}^{L_z} \left\{ \sum_{r_{ij}} |\log[C_{xy}(r_{ij},k)] - 2H_m \log(r_{ij}) - \log[C_1^{(xy)}]| \right\}, \tag{19}$$

$$E_C^{(z,r)} = \sum_{i=1}^{L_x} \sum_{j=1}^{L_y} \left\{ \sum_{r_k} |\log[C_z(i,j,r_k)] - 2H_m \log(r_k) - \log[C_1^{(z)}]| \right\}, \tag{20}$$

where H_m is the Hurst exponent estimated based on the measured data. Then

$$E_\phi = W_{Q_\phi} E_{Q_\phi} + W_w E_w + W_{C_\phi}^{(xy)} E_{C_\phi}^{(xy,r)} + W_{C_\phi}^{(z)} E_{C_\phi}^{(z,r)} \tag{21}$$

and

$$E_k = W_{Q_k} E_{Q_k} + W_{C_k}^{(xy)} E_{C_k}^{(xy,r)} + W_{C_k}^{(z)} E_{C_k}^{(z,r)}. \tag{22}$$

For the results that are described below, we used $C_1^{(z)}/C_1^{(xy)} = 5$.

If the extent of the correlations is up to a distance $r = \ell$, beyond which the ϕ and k values become uncorrelated with their data along the wells, then the correlation functions are given by

$$C_{xy}(r) = \begin{cases} C_1^{(xy)} r^{2H}, & r \leqslant \ell, \\ C_1^{(xy)} \ell^{2H}, & r > \ell, \end{cases} \tag{23}$$

and similarly for $C_z(r)$. The energy function for the correlations is then given by $E_C \simeq E_C^{(xy,r)} + E_C^{(xy,\ell)} + E_C^{(z,r)} + E_C^{(z,\ell)}$, in which we use expressions similar to Eqs. (19) and (20) for the four energy functions. The total energy functions for ϕ and k are then given by

$$E_\phi = W_{Q_\phi} E_{Q_\phi} + W_w E_w + W_{C_\phi}^{(xy,r)} E_{C_\phi}^{(xy,r)} + W_{C_\phi}^{(xy,\ell)} E_{C_\phi}^{(xy,\ell)} + W_{C_\phi}^{(z,r)} E_{C_\phi}^{(z,r)} + W_{C_\phi}^{(z,\ell)} E_{C_\phi}^{(z,\ell)} \tag{24}$$

and

$$E_k = W_{Q_k} E_{Q_k} + W_{C_k}^{(xy,r)} E_{C_k}^{(xy,r)} + W_{C_k}^{(xy,\ell)} E_{C_k}^{(xy,\ell)} + W_{C_k}^{(z,r)} E_{C_k}^{(z,r)} + W_{C_k}^{(z,\ell)} E_{C_k}^{(z,\ell)}. \tag{25}$$

As before, each of the weight factors is inversely proportional to the average change of its corresponding energy function. For the results described below, the cutoff length ℓ is one-third of the medium's linear size, $\ell = \frac{1}{3}L$.

Let $B(i)$ be the value attributed to block i of the grid. After a few SA iterations that changes $B(i)$, there is no guarantee that $B(i)$ will be in the ranges in which ϕ (k) should vary. Thus we define $B_\phi(i)[B_k(i)]$ to be the block value that varies during the optimization process and is required to follow the specified correlation function. Then, $\phi(i)[k(i)]$, the *actual* porosity (permeability) of block i, is related to $B_\phi(i)$ $[B_k(i)]$ by

$$\phi(i) = \frac{B_\phi(i) - B_{\phi_m}}{B_{\phi_M} - B_{\phi_m}} (\phi_M - \phi_m) + \phi_m \tag{26}$$

and

$$k(i) = \frac{B_k(i) - B_{k_m}}{B_{k_M} - B_{k_m}} (k_M - k_m) + k_m, \tag{27}$$

where (ϕ_M, k_M) and (ϕ_m, k_m) are, respectively, the maximum and minimum values of ϕ and k that we expect the porous medium to have (estimated from the ϕ and k data and other types of geological information about the porous formation), and (B_{ϕ_M}, B_{k_M}) and (B_{ϕ_m}, B_{k_m}) are the corresponding values of the SA variables $B_\phi(i)$ and $B_k(i)$ in the entire system for every iteration.

Let us note that during the SA iterations the quantities (B_{ϕ_M}, B_{k_M}) and (B_{ϕ_m}, B_{k_m}) are random variables. However, as the distributions of ϕ and k approach their optimal form, these quantities take on constant values that no longer change with further SA iterations. As a result, the optimal distributions of ϕ and k contain the correct correlation functions and structures.

V. THE OPTIMIZATION PROCESS

The computations for *simultaneous* determination of the optimal spatial distributions of ϕ and k are carried out as follows.

(1) The weight factors are estimated.

(2) Synthetic distributions of ϕ and k are generated, and the results along the five wells are taken as the "data." The rest will be used later on for comparison with the optimal values.

(3) Using the synthetic distributions, we solve Eqs. (1) and (8) in order to compute the FA times at the specified receivers and the time-dependence of the fluid's production rates. These are then taken as the data. We denote by $Q_\phi^{(m)} \times(t)$ the synthetic data for the rates of the fluid production when the porosities are varied during the optimization process, and by $Q_k^{(m)}(t)$ when the permeabilities are changed in the calculation of the corresponding energy function E_k. We also use the initial synthetic distributions to carry out simulation of two-phase flow (see below) in the porous medium, the results of which will be compared later with those obtained with the optimal distributions.

(4) Selecting from a Gaussian distribution, we distribute the $B_\phi(i)$ and $B_k(i)$ values in the grid blocks for which the ϕ and k values are not known (in the interwell zones). The corresponding values of ϕ, k, and $K(\phi)$ are then computed.

(5) Equation (1) is solved, and the FA times t_s are computed for all the grid blocks.

(6) Equation (8) is solved, and the production flow rates are computed. The results for $t \leqslant t_{\max}$ are used in the optimization (when the optimal distributions are obtained, the production flow rates are computed for $t > t_{\max}$ in order to test the accuracy of the distributions. In all the cases, $t_{\max} = 20$ days. We denote by $Q_\phi^{(s)}(t)$ the results when ϕ is varied, and by $Q_k^{(s)}(t)$ when k is varied in the calculation of E_k. [Note that, for the first step of the optimization process, this is already accomplished in step (3) described above.]

(7) The correlation functions $C_\phi(r)$ of the spatial distribution of ϕ are computed. Certain tricks are used [1,24] to speed up the computations.

(8) The correlation functions $C_k(r)$ of the spatial distribution of k are also computed by a method similar to step (7).

(9) The initial energy functions E_ϕ(old) and E_k(old) are computed, their values are normalized to one, and the initial "temperature" T_0 is set to be $T_0 = 1$.

(10) A block i of the computational grid is selected at random, and a direction—x, y, or z—is also chosen with equal probabilities. Then the $B_\phi(i)$ associated with block i is changed by

$$B_\phi^{\text{new}}(i) = B_\phi(i+1) + r, \tag{28}$$

or

$$B_\phi^{\text{new}}(i) = B_\phi(i-1) + r, \tag{29}$$

with equal probabilities, where r is a random number selected from a Gaussian distribution with unit variance. We found [24] this choice of r to result in accurate FBM arrays with good computational efficiency. $B_\phi(i \pm 1)$ represent the block values along the selected direction that are neighbors of the block represented by $B_\phi(i)$. Equations (28) and (29) are motivated by the fact that, as mentioned earlier, the successive increments in a FBM array follow a Gaussian distri-

bution, and selecting r from this distribution ensures that this property is automatically built into the array.

The corresponding porosity $\phi(i)$ is then computed. Note that Eqs. (28) and (29) imply that the porosity $\phi(i)$ of block i changes according to

$$\phi_{\text{new}}(i) = \phi(i+1) + \frac{\phi_M - \phi_m}{B_{\phi_M} - B_{\phi_m}} r, \tag{30}$$

or

$$\phi_{\text{new}}(i) = \phi(i-1) + \frac{\phi_M - \phi_m}{B_{\phi_M} - B_{\phi_m}} r, \tag{31}$$

which ensure that the final optimal porosity distribution will have the correct correlation function, and that if the randomly selected block i lies along the wells for which porosity data are available, the value of $B_\phi(i)$ will be changed by the SA iteration, but $\phi(i)$ will not, hence honoring (preserving) the data.

(11) Steps (5)–(7) are carried out and the new energy, E_ϕ(new), and the change in the energy, $\Delta E_\phi = E_\phi(\text{new}) - E_\phi(\text{old})$, are computed. If $E_\phi(\text{new}) < E_\phi(\text{old})$, the change is accepted and we set $E_\phi(\text{old}) = E_\phi(\text{new})$. If $E_\phi(\text{new}) > E_\phi(\text{old})$, the change is accepted or rejected using the Metropolis algorithm [i.e., based on a probability proportional to the Boltzmann's factor, $\exp(-\Delta E_\phi / T)$]. If in this case the change is accepted, we set $E_\phi(\text{old}) = E_\phi(\text{new})$.

(12) A block i' in the computational grid is selected at random, and a direction—x, y, or z—is also chosen with equal probabilities. Then, the $B_k(i')$ associated with the block is changed. The algorithm for doing so is the same as in step (10).

(13) Steps (6) and (8) are carried out and the new energy, E_k(new), and the change in the energy, $\Delta E_k = E_k(\text{new}) - E_k(\text{old})$, are computed. The change in the block's permeability is accepted or rejected according to the algorithm described in step (11).

In addition, we also set a maximum number of iterations for each temperature, and a maximum cumulative total change in the energy for E_ϕ and E_k. When the number of accepted energy changes reaches a suitable, *a priori* specified number, or when the maximum allowed changes in the energy are reached or exceeded, step (14) described below is undertaken. Otherwise, we go back to step (10). Typically, at the initial steps of the SA process (at high temperatures) the accepted changes are achieved before the maximum allowed change is reached or exceeded. At very low temperatures, on the other hand, the maximum allowed changes in the energy are reached before the accepted number of changes attains its prespecified number, as the number of rejections are large at such temperatures.

(14) The temperature is lowered according to the schedule, $T_{\text{new}} = 0.9 T_{\text{old}}$.

(15) We also test for convergence to the optimal distributions. If, for any iteration, ΔE_ϕ and ΔE_k are less than some prespecified values the iteration is terminated. If not, the temperature is lowered according to the above schedule (after a suitable number of accepted changes is obtained, or if the maximum allowed change is reached or exceeded) and the iteration process is continued. The total number of iterations for achieving convergence depends on the system's size and the value of the Hurst exponent H.

VI. TWO-PHASE FLOW COMPUTATIONS

To further test the computed optimal distributions of ϕ and k, we also carry out the simulation of two-phase flow in the model porous medium. We simulate the classical problem in which water is injected into a porous medium to displace the oil there. The oil is produced through another well. The injection and production wells are the same as those for the PT simulation described in Sec. III.

Combining the Darcy's law and the mass conservation equation yields the following equations for flow of oil and water in a 3D porous medium:

$$B_o^{-1} \nabla \cdot (k \lambda_o \nabla \Phi_o) - \frac{q_o}{\rho_o} = \frac{\partial}{\partial t}\left(\frac{\phi S_o}{B_o} \right), \tag{32}$$

$$B_w^{-1} \nabla \cdot (k \lambda_w \nabla \Phi_w) - \frac{q_w}{\rho_w} = \frac{\partial}{\partial t}\left(\frac{\phi S_w}{B_w} \right), \tag{33}$$

where $\Phi_w = P_o - P_c - \rho_w g h$, and $\Phi_o = P_o - \rho_o g h$, with $P_c = P_o - P_w$, P_o and P_w being the pressures in the oil and water phases. λ_o and λ_w are, respectively, the mobility of the oil and water (the mobility of a fluid is defined as the ratio of its permeability and viscosity), S_w and $S_o = 1 - S_w$ their corresponding saturations (the pore volume fraction that they occupy), (B_o, q_o) and (B_w, q_w) the corresponding formation volume factors and flow rates, and h is a grid block's (center's) depth from the sea level. We then combine Eqs. (32) and (33) to obtain a single equation for P_o which contains no explicit time derivatives of the fluids' saturations:

$$B_o \left[\nabla \cdot \left(k \frac{\lambda_o}{B_o} \nabla P_o \right) - \rho_0 g - \frac{q_o}{\rho_o} \right] + B_w \left\{ \nabla \cdot \left[k \frac{\lambda_w}{B_w} (\nabla P_o - \nabla P_c) \right] - \rho_w g - \frac{q_w}{\rho_w} \right\} = \phi C \frac{\partial P_o}{\partial t}, \tag{34}$$

where $C_i = -B_i^{-1} \partial B_i / \partial P_i$ $(i = o, w)$ represents the fluids' compressibility, $C_r = -\phi^{-1} \partial \phi / \partial P_o$ is the rock's compressibility, $C = C_r + C_o S_o + C_w S_w$, and the terms $\rho_o g$ and $\rho_w g$, representing the gravitational terms, operate only in the z (vertical) direction.

The governing equations for P_o and S_o are solved by a FD method. The oil pressure in any block is represented by an average value attributed to its center. Likewise, the flow rates q_o and q_w are assumed to represent the average rates in any gridblock. The time derivative is approximated by a suitable FD form, such as $C\phi(P_i^{n+1} - P_i^n)/\Delta t$, if we use a forward FD approximation, where P_i^n is the pressure after n time steps at grid point i representing a block, and Δt is the time step. The simulator first solves the governing equations for the pressure P_o, and then computes the oil saturation S_o by solving Eq. (32). To obtain the solution, we use a combination of the so-called implicit pressure-explicit saturation (IMPES) method [25] which discretizes the equations for P_o by an

implicit FD method, and the equation for S_o by an explicit FD scheme. The injection and production wells are represented as described in Sec. III B, using equations similar to Eq. (9).

The largest variations in S_o and P_o occur in the near-well regions, which also control the maximum allowed time step Δt when the flood front is close to them. Therefore, at the beginning of the injection, Δt must be small, but when the front is no longer near the injection well, it can be much larger. When the front reaches the vicinity of the production well, Δt must again be small. Therefore in a small zone of grid blocks around the wells we use the fully implicit FD method for discretizing the governing equations, while the IMPES method is used in the remaining part of the grid. The reason for using a combination of the two methods is as follows.

The IMPES method is conditionally stable and converges to the correct solution if the time step Δt is selected carefully. We imposed the condition that the S_o and P_o changes in any grid block between two consecutive time steps must remain tightly bounded, by adjusting Δt such that the $S_o P_o$ changes between t and $t+\Delta t$ in any grid block were, respectively, no more than 0.05 and 100 psi. In addition, an adaptive time-step method was used. The limitations of the IMPES method are that (a) because a large portion of the porous medium far from the wells may experience very slow changes in P_o and S_o, it is not efficient to use very small Δt, and (b) the method is not accurate if large variations in the dependent variables occur rapidly. The time-truncation errors are generally larger in implicit simulators. A fully implicit method provides the required stability, but at a considerably higher computational cost.

For the fully implicit part, we guess the S_o distribution at time t and solve the discretized equations for P_o. The S_o distribution is then computed based on the newly calculated P_o distribution. The procedure is iterated several times until converged solutions are obtained. For the IMPES part, after computing the P_o distribution after each time step, we solve Eq. (32) in which the time-derivative term is discretized explicitly. In both cases the discretized equations are solved by a combination of the Newton-Raphson and biconjugate-gradient methods. The boundary conditions are a constant water flow rate at the injection well, and a constant bottom-hole pressure at the production well. The initial pressure of the porous medium is assumed to be constant everywhere. These are the conditions for simulation of a typical displacement of oil by water in an oil reservoir. The simulations are carried out for a period of 3000 days, a typical period for practical applications. We must emphasize that no data for the two-phase flow problem are used in the optimization process.

To carry out the simulations, one must specify the relative permeability curves and their dependence on the saturation of the fluids. The relative permeability k_{ri} of a fluid i is the ratio of the permeability of that part of the pore space occupied by the fluid and the single-phase permeability k of the block [4,14]. For the computations reported in this paper, we used the following equations:

$$k_{rw} = \left(\frac{S - S_{wc}}{1 - S_{wc} - S_{or}} \right)^2, \tag{35}$$

$$k_{ro} = \left(\frac{1 - S - S_{or}}{1 - S_{wc} - S_{or}} \right)^2, \tag{36}$$

with the residual and irreducible saturations of the water and oil phases being $S_{wc}=S_{wi}=S_{or}=0.2$. The complete details of all the computations are given elsewhere [26].

VII. RESULTS

To test the accuracy of the computed optimal distributions of ϕ and k, we proceed as follows. Synthetic spatial distributions of ϕ and k are generated and assigned to the grid blocks. The synthetic permeabilities vary over three orders of magnitude, hence giving rise to a broad distribution and providing a stringent test for the optimization problem. The porosities vary in the range (0,0.5), the typical range for many natural porous media. We then take the synthetic ϕ and k values along the wells, as well as the computed FA times at the receivers and the fluid's production rates up to a maximum time $t_{\max}$ (using the synthetic ϕ and k values), as the "data" to be utilized in the optimization process. The rest of the synthetic ϕ and k values, as well as the computed FA times, the fluid's production rates for times $t > t_{\max}$, and the two-phase flow predictions using the synthetic data are set aside to be compared later with those computed based on the optimal distributions of ϕ and k.

We first describe and discuss the results for the case in which we use a point source for the seismic waves at the computational grid's center. Figure 1 presents the comparison between the actual synthetic data and those computed by the optimization method. The Hurst exponents for the ϕ and k data are $H_\phi=0.3$ and $H_k=0.7$. To obtain a better sense for the accuracy of the optimal distributions, we computed the correlation coefficient R, defined by,

$$R = \frac{\sum_i [(X_i - \langle X \rangle)(Y_i - \langle Y \rangle)]}{\sqrt{\sum_i (X_i - \langle X \rangle)^2 \sum_i (Y_i - \langle Y \rangle)^2}}, \tag{37}$$

where X_i and Y_i are, respectively, the actual (synthetic) and computed optimal values of the quantity at grid block i, and $\langle X \rangle$ and $\langle Y \rangle$ are their averages. The results shown in Fig. 1 are for a single realization of the porous medium. All the computed FA times obtained with the optimal model nearly collapse onto the straight line, $Y=X$, where they are equal to the actual (synthetic) values, with a correlation coefficient $R=0.997$. As demonstrated in Part I, the same degree of accuracy is obtained for all the computed FA times in the optimal models, for all the cases that we considered and describe below. Hence we will not show the comparison of the FA times for the remaining cases that we describe below.

In Fig. 1, and for all other cases discussed below, only those optimal values of ϕ and k of the grid blocks for which no data were used in the optimization are compared with the synthetic data. As Fig. 1 indicates, the correlation coefficient R for the permeability results are higher than that for the porosities, indicating better overall agreement between the synthetic data and the predicted optimal ones. We will come

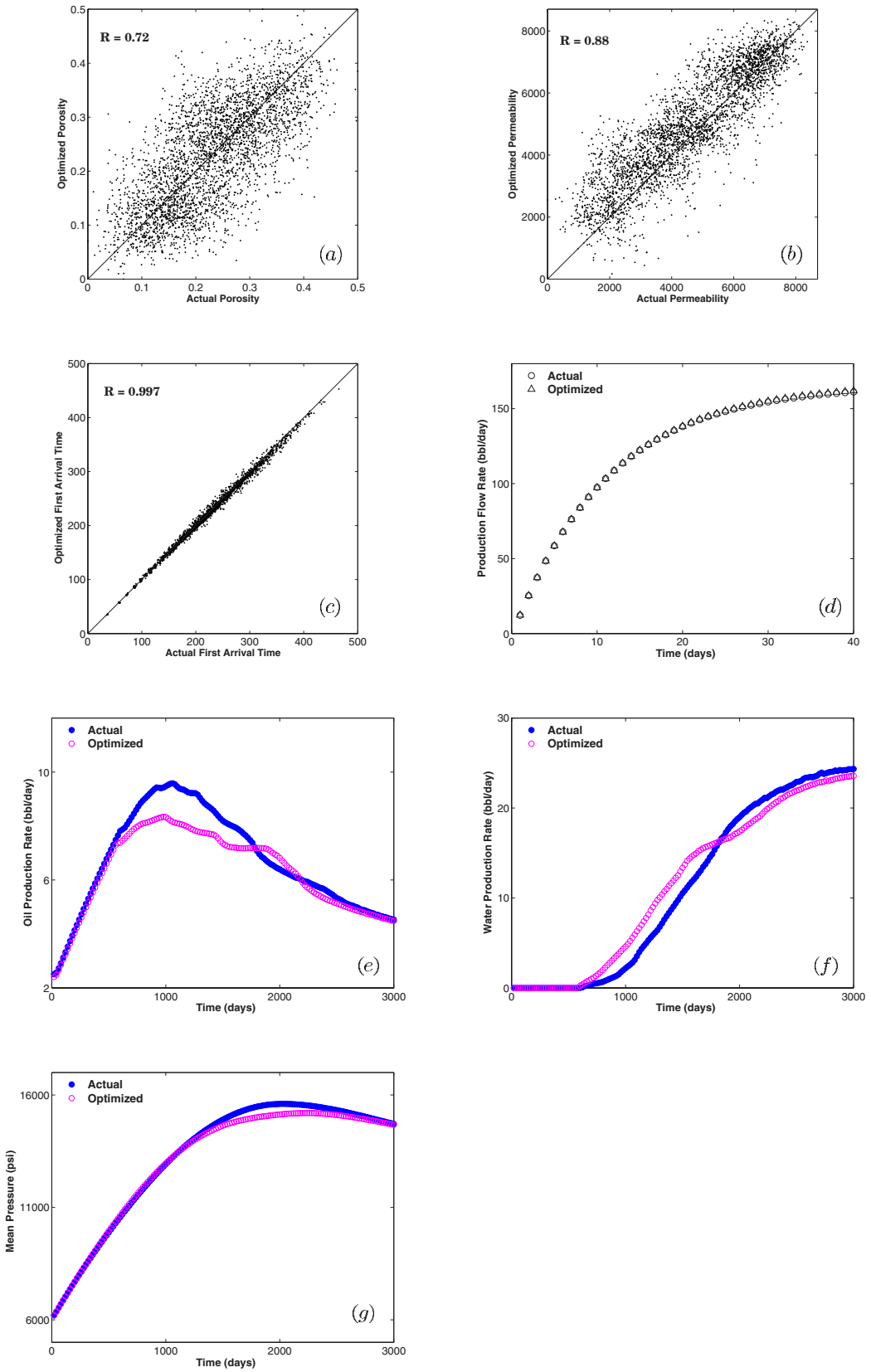

FIG. 1. (Color online) Comparison of the synthetic data with the predicted porosities (a); permeabilities (b); the first-arrival times (c); time-dependence of the pressure of a single fluid (d); the rates of oil (e) and water production in barrel (bbl) (f); and the mean pressure (g) in the optimal model of the porous medium. The seismic waves' source is at the medium's center, and the Hurst exponents of the porosity and permeability data are H_ϕ=0.3 and H_k=0.7. Note that in (d) the flow rates for only $t \leqslant 20$ days were used in the optimization. The rest of the optimized values shown represent predictions.

back to this point shortly. While the comparison between the optimal and actual values of ϕ and k shown in Figs. 1(a) and 1(b) exhibits some scatter, the comparison between the computed rates of production of a fluid in single-phase flow, obtained by solving Eq. (8) in the optimal model, and the actual synthetic data indicates excellent agreement. Note that the optimization process used the synthetic data for the production rates only up to the time $t=t_{\max}=20$ days. As Fig. 1(d) indicates, however, the agreement between the synthetic data and the predicted production rates with the optimal model beyond $t_{\max}$, *for which we used no data in the optimization process*, is still excellent.

A most stringent test of the model is its accuracy for *predicting* the properties of two-phase flows in the porous medium. We refer to these results as predictions because we used no two-phase flow data in the optimization process. From a practical viewpoint, the three most important quantities of interest for the two-phase flow (water flooding) problem that we solve are the rates of production of water and oil, and the mean pressure of the porous medium (or the oil reservoir). The comparison between the predicted values of the three quantities, computed with the optimal model, and the synthetic data is also shown in Figs. 1(e)–1(g). The predicted and actual mean pressures are in excellent agreement. The predicted water production rates are also in close agreement with the synthetic data. In particular, the breakthrough point, i.e., the time at which water is first produced at the production point (initially only oil is produced), is accurately predicted by the optimal model. Note that, from a practical viewpoint, the breakthrough point is, in fact, a most important property to be accurately predicted. As for the rate of oil production, all the important features of the actual data are nicely predicted by the optimal model. The quantitative agreement between the predictions and the synthetic data are actually excellent over much of the long period of time for which the simulations were carried out. Only the peak production is not predicted very accurately. However, note that these results are obtained with a single realization. As demonstrated in Part I, if a few realizations are made, the agreement between the averages of all the realizations and the data for all the properties shown in Fig. 1 will actually be very good.

Figure 2 compares the results for $H_\phi=0.7$ and $H_k=0.3$. In this case, the correlation coefficient for the ϕ values is much higher than that for the k values, which is the opposite of the results shown in Fig. 1. This is actually a general trend in all the cases that we have studied: the R values for the permeabilities are higher than those for the porosities, when the Hurst exponents $H_k>0.5$ and $H_\phi<0.5$, whereas the opposite is true when $H_k<0.5$ but $H_\phi>0.5$.

The agreement between the synthetic data and the predicted rates of production of a fluid in single-phase flow simulation, computed using the optimal model, is excellent, even for times beyond $t_{\max}$. Moreover, the agreement between the predictions for the two-phase flow problem and the results obtained with the actual synthetic data for ϕ and k also ranges from very good to excellent. All the trends in the data for the two-phase flow problem are predicted correctly by the optimal model, the breakthrough time. Only the peak oil production has been overestimated somewhat, as opposed to what is shown in Fig. 1 where it is underestimated. We have obtained [26] extensive results with similar accuracies for the cases in which the Hurst exponents H_k and H_ϕ are both above or below 0.5 and, therefore, do not present them here.

Let us now consider the case in which the seismic waves' source is a line, placed at the center of the computational grid in the vertical (z) direction. Figure 3 presents the results and compares them with the actual data, for the case for which $H_k=0.7$ and $H_\phi=0.3$. As pointed out earlier, when $H_k>0.5$, the correlation coefficient R for the k values is higher than those for the ϕ values, and Figs. 3(a) and 3(b) confirm this trend. Once again, the predicted rates of production of a fluid in single-phase flow in the optimal model are in excellent agreement with the synthetic data, even for times beyond $t_{\max}=20$ days. The same degree of accuracy is obtained for the predicted rates of water production in the two-phase flow problem. The predicted time-dependence of the porous medium's mean pressure is also in very good agreement with the synthetic results, deviating from them by no more than a few percent. In particular, the time at which the peak mean pressure is reached is predicted very accurately, a feature which is very important to practical applications. Similarly, the predicted rates of oil production are in good agreement with the synthetic results.

Figure 4 compares the computed predictions for all the quantities of interest with the synthetic data, for the case in which $H_k=H_\phi=0.7$. Once again, the agreement between the synthetic data and the predictions for the rates of production of a fluid in the single-phase flow simulations beyond $t_{\max}=20$ days, the rates of water and oil production in the two-phase flow, and the mean pressure of the porous medium is excellent. Similar results were obtained [26] for other values of H_k and H_ϕ and, therefore, are not shown.

We now present some sample results for the case in which the waves' source is planar and located on the top horizontal (xy) plane of the computational grid (representing the ground surface) in order to simulate a case similar to what is done in seismic exploration. Figure 5 compares the predictions for all the quantities that are of interest in practical applications with the synthetic data with $H_k=H_\phi=0.7$. All the trends in the synthetic data are predicted accurately by the optimal model.

Finally, Fig. 6 compares the predictions of the optimal model with the synthetic data, for the case in which there is a cutoff length scale ℓ in the correlation functions of the porosity and permeability data. The results shown in Fig. 6 were obtained with $H_k=0.7$ and $H_\phi=0.3$. The agreement between the numerical predictions and the synthetic data is excellent for all the properties that are important in practice, such as the rates of the oil and water production. One should also compare these results with those shown in Fig. 3, which were obtained for the same set of parameters, except that no cutoff length scale for the correlations in the ϕ and k data was introduced.

VIII. DISCUSSION: WHEN AND WHY DOES THE OPTIMIZATION METHOD WORK?

The success of the optimization method in providing accurate predictions for the two-phase flow problem motivates

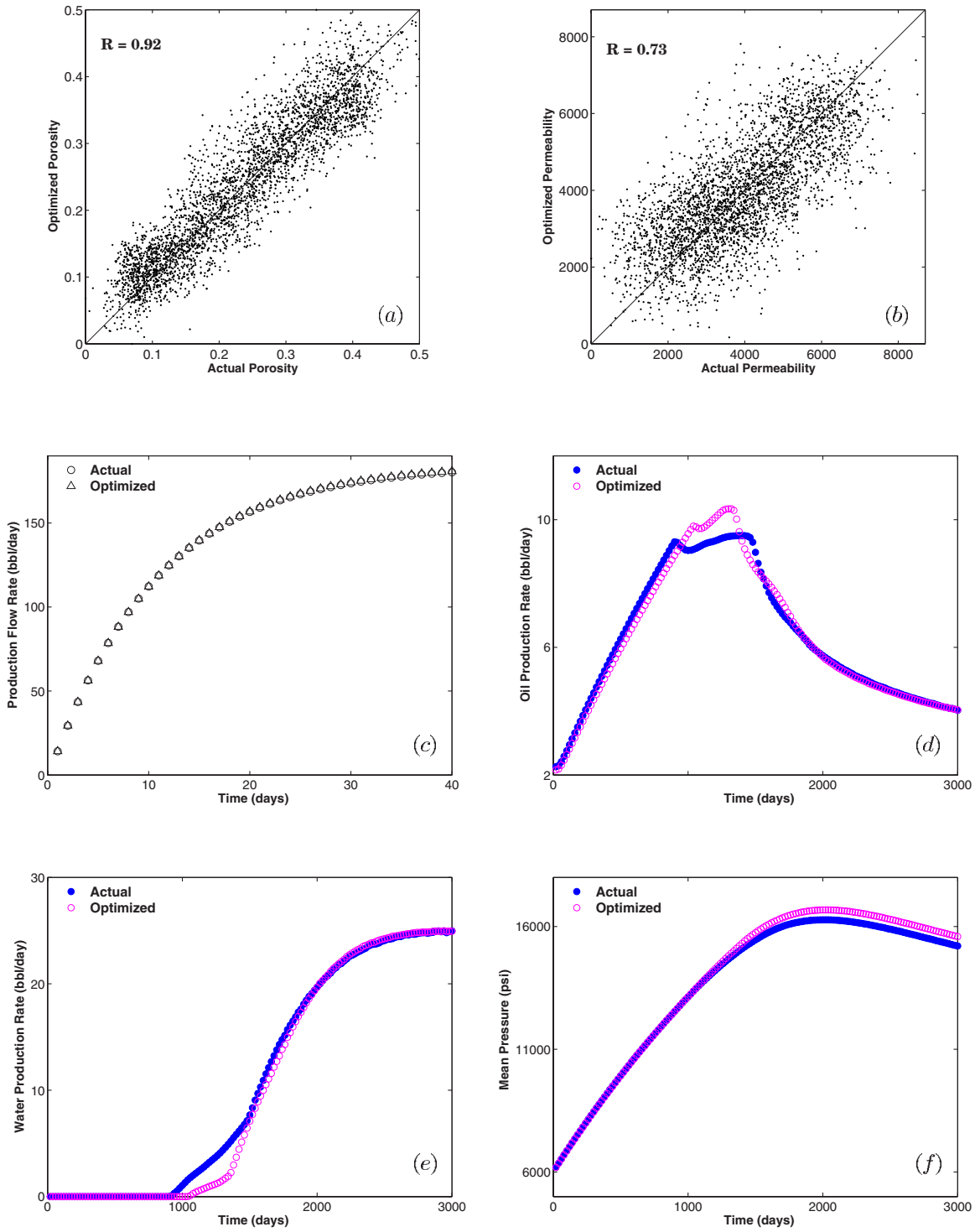

FIG. 2. (Color online) Comparison of the synthetic data with the predicted porosities (a); permeabilities (b); time-dependence of the pressure of a single fluid (c); the rates of oil (d) and water (e) production, and the mean pressure (f) in the optimal model of the porous medium. The seismic waves' source is at the medium's center, and the Hurst exponents of the porosity and permeability data are H_ϕ=0.7 and H_k=0.3. Note that in (c) the flow rates for only $t \leqslant 20$ days were used in the optimization. The rest of the optimized values shown represent predictions.

the following question: When can one expect the method to be successful, and at what computational cost? The efficiency of the computations is discussed in the next section and, therefore, in this section we address the first part of the question.

Let us first note the nontrivial nature of the method presented in this paper, as an extension of what we described in Part I. To obtain the optimal spatial distributions of ϕ and k, we must minimize, using the SA method, *two* distinct objective (or energy) functions, namely, E_ϕ and E_k. For Ising-like

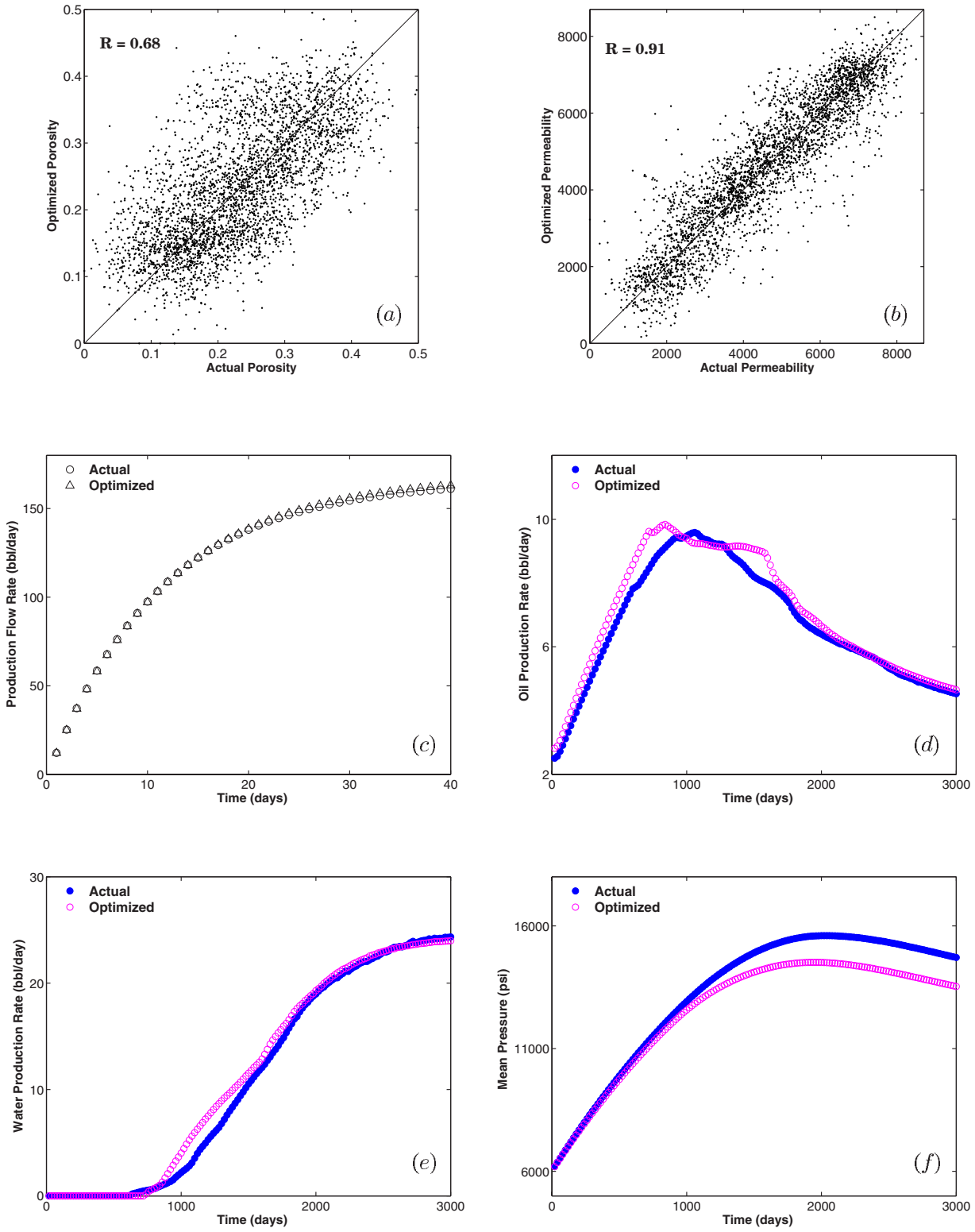

FIG. 3. (Color online) Same as in Fig. 2, but with the waves's source being the vertical line at the medium's center, and H_ϕ=0.3 and H_k=0.7.

problems, for example, one obtains [27] *one* ensemble of spins with definite macroscopic properties. In the present problem, we obtain one ensemble of the ϕ values and another ensemble for the k values, both of which satisfy stringent constraints imposed by the data.

As described above, the optimization method has several ingredients, each of which contributes to the success or failure of the method. However, the most important three ingredients are as follows.

(i) *The temperature schedule*. The SA method can become

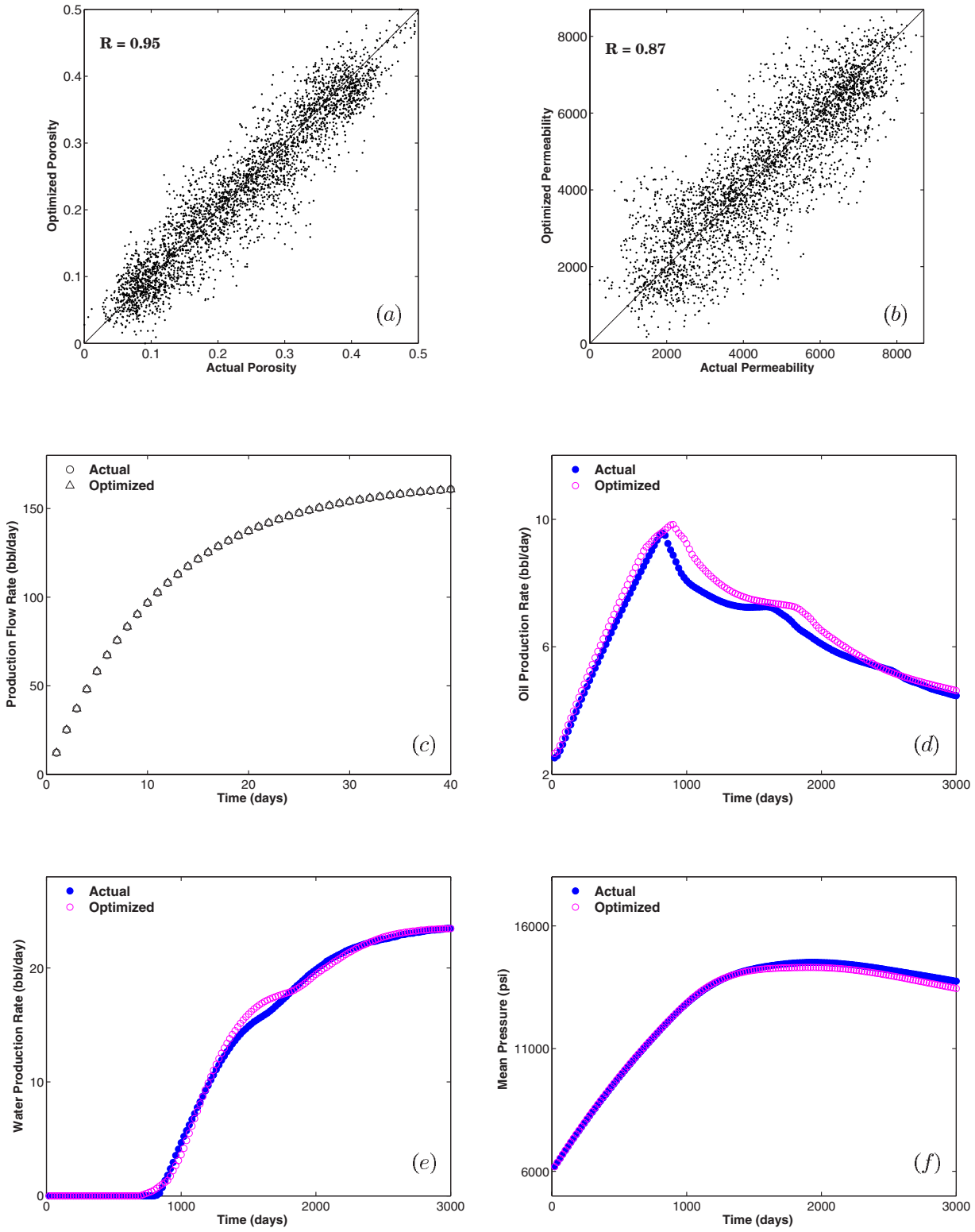

FIG. 4. (Color online) Same as in Fig. 2, but with the waves' source being the line at the medium's center in the vertical direction, and $H_\phi = H_k = 0.7$.

extremely time-consuming if it is utilized in a "brute force" manner. It is clear that the key ingredient to the success or failure of the method is the ability to decide the accuracy of the computed distributions between two successive SA iterations, and whether to accept the perturbation that resulted in the most recent distributions [28]. However, as described above, not all the perturbations that *increase* the value of the objective functions are automatically rejected. Otherwise, the energy function might become trapped in a local minimum. At high temperatures, the probability that an unfavorable

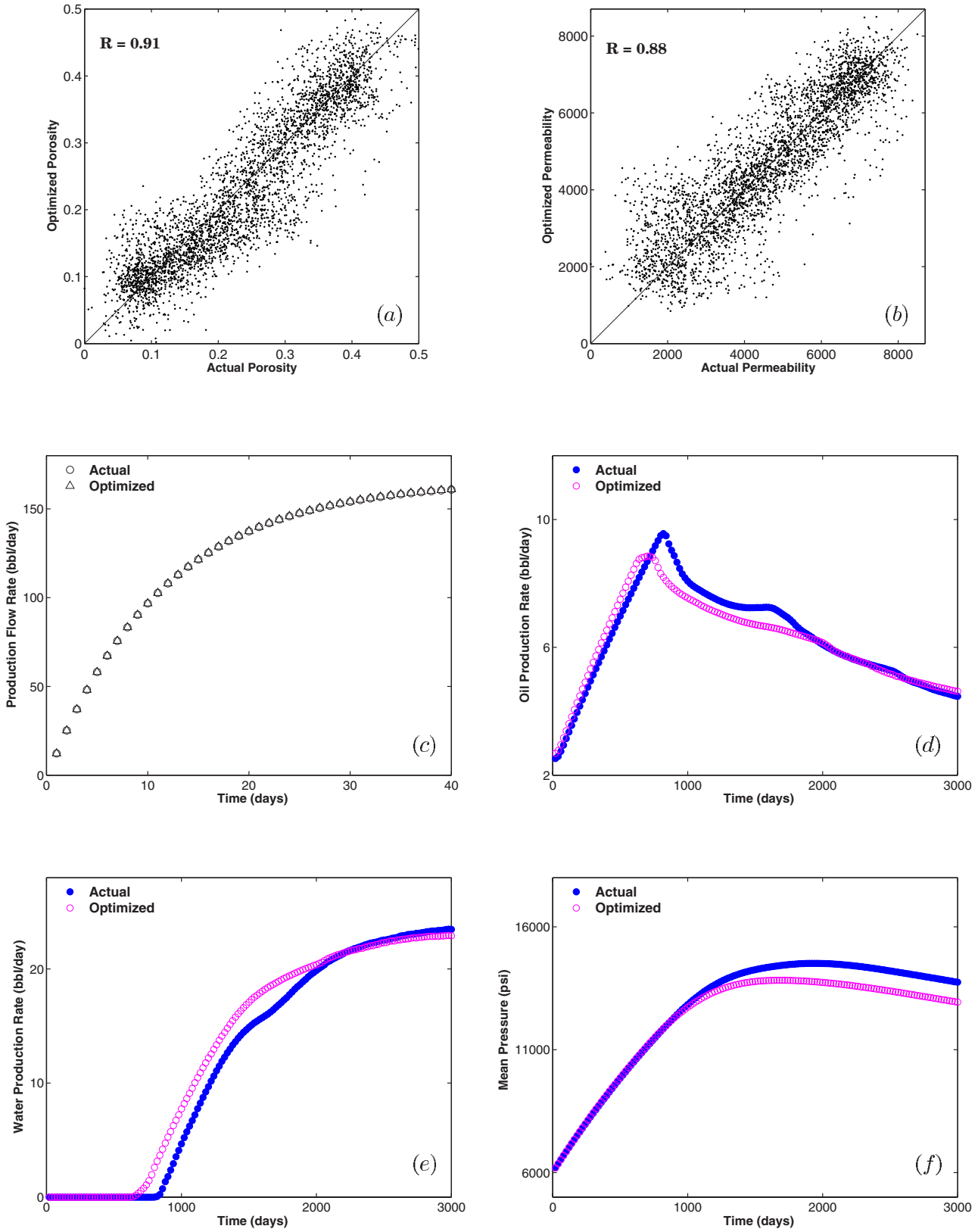

FIG. 5. (Color online) Same as in Fig. 2, but with the waves' source being planar on the top (xy) plane of the grid, and $H_\phi = H_k = 0.7$.

perturbation is accepted is greater. Therefore the success of the SA method depends critically on the *cooling rate* of the realizations which, in turn, depends on the temperature schedule that one utilizes. If the cooling rate is too high, the method will fail. If it is too low, the method will converge, but the time to converge will be prohibitively long. As a result, the choice of a suitable temperature schedule, by

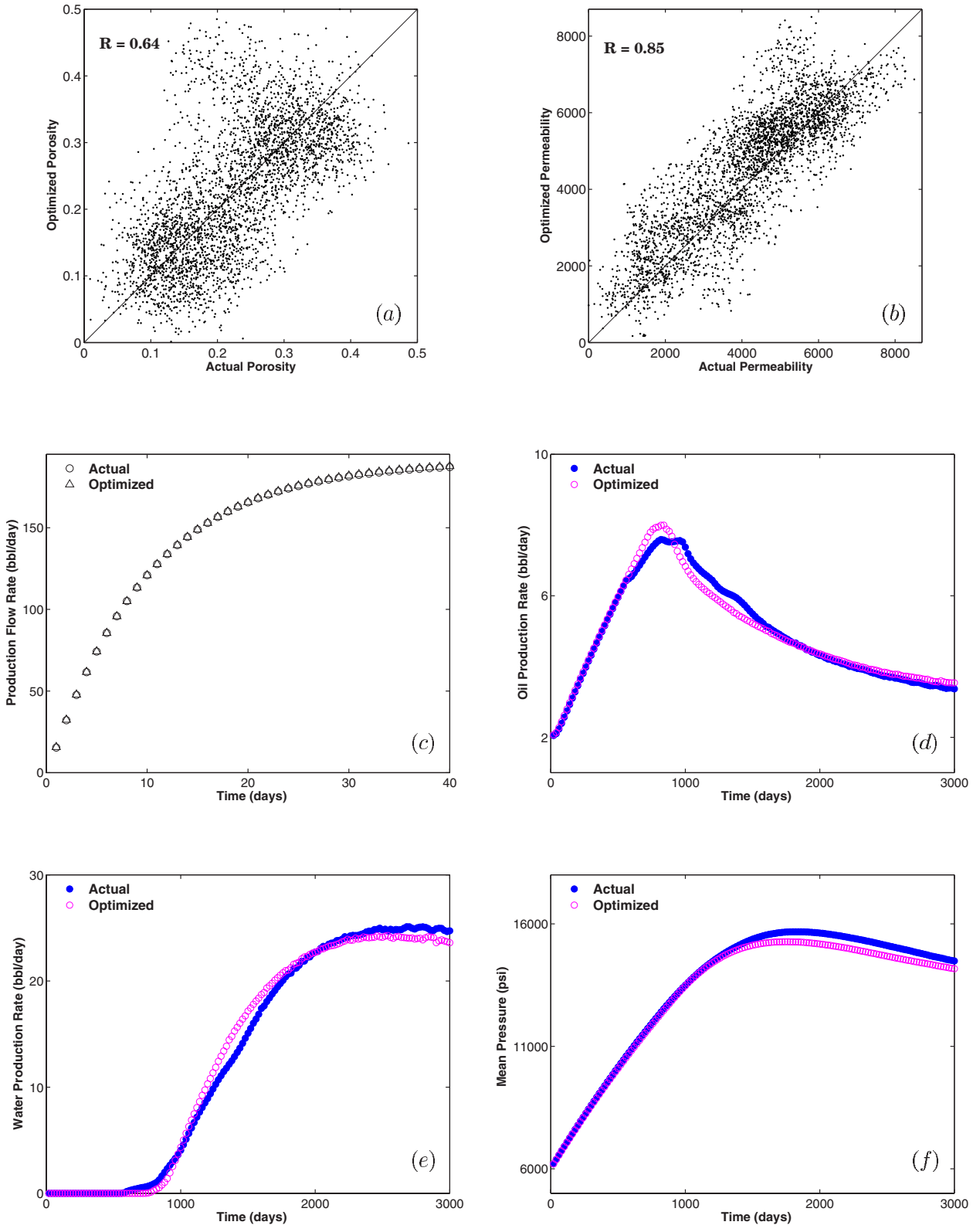

FIG. 6. (Color online) Same as in Fig. 2, but with the waves's source being the vertical line in the middle of the computational grid, and a cutoff length scale ℓ for the ϕ and k correlations which is one-third of the medium's linear size, with H_ϕ=0.3 and H_k=0.7.

which the system is cooled off, is crucial to the method's success.

Theoretically, if we utilize the temperature schedule, $T_k = T_0/\ln(k)$, the convergence will be guaranteed [29]. However, such a temperature schedule is too slow and impractical. In practice, empirical schedules, such as what we used, $T_k=(0.9)^k T_0$, are utilized that have proven to be highly effective in yielding fast convergence [30].

(ii) *The weights W*. As Eqs. (21), (22), (24), and (25) indicate, each total energy function consists of several terms, each of which represents the contribution of one segment of the data that the optimal distributions must satisfy, and each is weighted by its own weight factor. The weight factors are *not* equal. They are estimated such that, on average, each component of the total energy functions contributes equally to their changes during the SA iterations, which explains Eqs. (15) and (16). The weights cannot be calculated analytically. Therefore *a priori* proper estimation of the weight factors is another crucial aspect of accurate and efficient optimization.

(iii) *Complexity of the energy function*. The optimal spatial distributions of ϕ and k that we determine by the SA method represent only two of a very large ensemble of the possible ϕ and k distributions that have the same desirable properties, namely, that they yield the correct FA times at certain locations; the correct production flow rates; the correct correlation properties of ϕ and k, and honor the existing data for them. What this implies is that if we equilibrate the system at each temperature and use slow cooling, the desired distributions will be obtained.

However, this happens only if the energy function is not too complex. If there are too many constraints that the total energy functions must satisfy, then the probability of obtaining convergence to the true optimal distributions of ϕ and k (the true global minima of the total energy functions) would be relatively small. That is not, however, the case in the problem that we consider, since the permeabilities and porosities are related (albeit through a relation the exact form of which is unknown).

IX. THE EFFICIENCY OF THE COMPUTATIONS

One must address three important questions regarding the efficiency and practicability of the optimization method described in this paper and Part I. They are (a) how fast are the above computations carried out? (b) How does the computation time scale with the size of the grid representing a porous medium, or with the number of variables to be optimized, and (c) can the optimization method developed in this paper be used in practice for modeling of large-scale porous media?

For concreteness, consider modeling of an oil reservoir. In our computations we used a grid that contained $15 \times 15 \times 15$ blocks. Hence we optimized the porosities and permeabilities of about 3300 grid blocks. In practice, the typical grid that is used in the simulation of fluid flow through an oil reservoir contains *at most* 15 000–20 000 grid blocks, which is greater than the grid that we used in our computations by a factor of only about 5 to 6. We also point out that about 95% of the total computation time is spent for solving repeatedly Eqs. (1) and (8) during the SA trials.

Note that numerical simulation of Eqs. (1) and (8) can be done in completely parallel mode, as the waves' amplitude ψ and the fluid pressure P are not directly linked. Their only link is through the porosity, but once the grid blocks' porosities are specified, Eqs. (1) and (8) become decoupled. Thus we provide estimates for the computation times with a computer with only two processors. The total computation times for the grid that we used in our calculation is about 2.4 CPU days or less on a SUN AMD Opteron workstation with two processors (such machines can have up to six processors). Because the computations are dominated by the times needed for solving Eqs. (1) and (8) repeatedly during the SA iterations, we need to know how such times scale with the grid size. As mentioned earlier, we use a fully explicit finite-difference approximation for discretizing Eq. (1). Therefore computing its numerical solution does not involve any iterative scheme. Instead, one marches forward, starting from the grid blocks around the wave source, and computes the waves' amplitudes ψ grid block by grid block. This implies that the time for computing the solution of Eq. (1) scales *linearly* with N, the number of grid blocks.

Moreover, Eq. (8), when discretized by the fully implicit FD approximation, is solved by the biconjugate-gradient (BCG) method. The computation time of the BCG method scales essentially linearly with N. (Strictly speaking, the computation time of the BCG method scales [30] with N as $N \ln N$). Thus under these conditions, the computation times for solving both Eqs. (1) and (8) scale linearly with the grid size. Therefore for a grid that contains about 20 000 blocks, the time for computing the optimal ϕ and k distributions is about 14 CPU days on a dedicated SUN workstation with two processors, which is acceptable and practicable.

We also point out that we have made no attempt to optimize the methods that we use for obtaining the numerical solutions of Eqs. (1) and (8). If this is done, the optimization process will be carried out more efficiently. Consider, for example, the fact that after each SA iteration we change the ϕ and k values for *at most* two blocks (one for ϕ and one for k). The rest of the grid remains intact. Therefore the solutions of Eqs. (1) and (8) before and after the perturbations in the ϕ and k values should not differ significantly in most of the grid. They should differ only slightly around the one or two blocks where ϕ and k were perturbed by the SA method. This is particularly true when the grid size is on the order of the size used in the modeling and simulation of oil reservoirs. One should, therefore, be able to take advantage of this fact and develop a scheme whereby, after each SA iteration, the waves' amplitudes and the fluid's pressure at only a small fraction of the grid blocks are updated, with the rest remaining intact.

Fast algorithms have been developed for the numerical simulation of Eq. (1) [31] if the equations are discretized by the FD approximation, as we do in this paper (see Part I and references therein). These algorithms carry out the parallelization based on the domain-decomposition method, while the communications between the nodes are performed by using the message passing interface strategy. They have been fast enough to allow the numerical simulation of Eq. (1) on a grid as large as 500^3 [32]. Given that, as we pointed out above, determining the numerical solutions of Eqs. (1) and (8) takes nearly 95% of the total computation time in the optimization method, these algorithms greatly facilitate the use of computational grids that are much larger than what we are discussing here.

One may be able to make the computations even more efficient by the following scheme. One does not attempt to

determine the optimal values of ϕ and k for every block of the computational grid. Instead, one determines the optimal values of ϕ and k for only those blocks that are around where one has numerical data, such as where the ϕ and k values are known, where the FA times have been recorded, and where the injection and production wells are located. The ϕ and k values for the rest of the blocks are determined by an accurate and deterministic method, such as kriging [4,14,21]. This may drastically decrease the number of variables to be optimized (hence resulting in very fast computations), yet yield accurate results. The preliminary results based on this idea have been very encouraging [33].

X. SUMMARY

For most large-scale porous media, such as oil reservoirs, there are usually limited data for the porosity ϕ and permeability k, whereas there are extensive data for the first-arrival times of seismic waves at certain receivers, as well as the time-dependence (history) of the pressure of a single fluid flowing in the porous formation (usually referred to as the pressure-transient data). Extending the method developed in Part I, we developed in this paper a method that utilizes such data for computing the optimal spatial distributions of ϕ and k. We assumed that the propagation of seismic waves in a large-scale porous medium is described by the acoustic wave equation [Eq. (1)], while the pressure-transient behavior of the fluid is described by a type of diffusion equation [Eq. (8)]. We showed that (a) if efficient numerical simulators, that solve Eqs. (1) and (8) and provide estimates of the fluid's time-dependent pressure and the FA times of the waves at a certain number of receivers, are linked with (b) a simulator that utilizes the simulated-annealing method (or any other efficient energy minimization technique, such as the genetic algorithm) and the data for the FA times and the fluid's pressure, together with limited data for the porosities and permeabilities of the porous medium, one can compute accurate optimal spatial distributions of ϕ and k. Such optimal distribution not only honors (preserves) all the data used in the optimization, but also provides accurate *predictions* for the important properties of flow of a single fluid, as well as flow of two immiscible fluids in the porous medium for which we used *no data* in the optimization.

ACKNOWLEDGMENT

The work of H. H. and M. R. R. was supported by the NIOC.

[1] H. Hamzehpour and M. Sahimi, Phys. Rev. E **74**, 026308 (2006).
[2] P. M. Adler, *Porous Media: Geometry and Transport* (Butterworth-Heinemann, Boston, 1992); P. M. Adler and J.-F. Thovert, *Fractures and Fracture Networks* (Kluwer, Dordrecht, 1999).
[3] H. H. Hardy and R. A. Beier, *Fractals in Reservoir Engineering* (World Scientific, Singapore, 1994).
[4] M. Sahimi, Rev. Mod. Phys. **65**, 1393 (1993); *Flow and Transport in Porous Media and Fractured Rock* (VCH, Weinheim, Germany, 1995).
[5] S. Kirkpatrick, C. D. Gellat, Jr., and M. P. Vecchi, Science **220**, 671 (1983).
[6] J. W. Cahn, J. Chem. Phys. **42**, 93 (1965).
[7] J. A. Quiblier, J. Colloid Interface Sci. **98**, 84 (1984); N. F. Berk, Phys. Rev. Lett. **58**, 2718 (1987); Phys. Rev. A **44**, 5069 (1991).
[8] J.-F. Thovert, F. Yousefian, P. Spanne, C. G. Jacquin, and P. M. Adler, Phys. Rev. E **63**, 061307 (2001), and references therein.
[9] A. P. Roberts and M. A. Knackstedt, Phys. Rev. E **54**, 2313 (1996).
[10] C. L. Y. Yeong and S. Torquato, Phys. Rev. E **57**, 495 (1997); **58**, 224 (1998); C. Manwart, S. Torquato, and R. Hilfer, *ibid.* **62**, 893 (2000).
[11] R. W. Mair, G. P. Wong, D. Hoffmann, M. D. Hürlimann, S. Patz, L. M. Schwartz, and R. L. Walsworth, Phys. Rev. Lett. **83**, 3324 (1999).
[12] See, for example, M. Sen and P. L. Stoffa, *Global Optimization Methods in Geophysical Inversion* (Elsevier, Amsterdam, 1995).
[13] D. Stauffer and A. Aharony, *Introduction to Percolation Theory*, 2nd ed. (Taylor and Francis, London, 1994); M. Sahimi, *Applications of Percolation Theory* (Taylor and Francis, London, 1994).
[14] J. R. Fanchi, *Principles of Applied Reservoir Simulation*, 2nd ed. (Gulf Professional Publishing, Houston, 2001).
[15] A. Ishimaru, *Wave Propagation and Scattering in Random Media* (Oxford University Press, Oxford, England, 1997); N. Bleistein, J. K. Cohen, and J. W. Stockwell, Jr., *Mathematics of Multidimensional Seismic Imaging, Migration, and Inversion* (Springer, New York, 2001).
[16] F. Gassmann, Vierteljahrsschr. Natforsch. Ges. Zur. **96**, 1 (1951).
[17] M. A. Knackstedt, C. H. Arns, and W. V. Pinczewski, Geophysics **68**, 1822 (2003).
[18] S. Torquato, *Random Heterogeneous Materials* (*Springer*, New York, 2002).
[19] M. Sahimi, *Heterogeneous Materials I* (Springer, New York, 2003).
[20] M. Krief, J. Garat, J. Stellingwerff, and J. Ventre, Log Analyst **31**, 355 (1990).
[21] C. V. Deutsch and A. G. Journel, *Geostatistical Software Library and User's Guide*, 2nd ed. (Oxford University Press, New York, 1998).
[22] F. Shahbazi, A. Bahraminasab, S. M. Vaez Allaei, M. Sahimi, and M. R. Rahimi Tabar, Phys. Rev. Lett. **94**, 165505 (2005); A. Bahraminasab, S. M. Vaez Allaei, F. Shahbazi, M. Sahimi, M. D. Niry, and M. R. Rahimi Tabar, Phys. Rev. B **75**, 064301 (2007).
[23] M. Sahimi and S. E. Tajer, Phys. Rev. E **71**, 046301 (2005); S. M. Vaez Allaei and M. Sahimi, Phys. Rev. Lett. **96**, 075507 (2006); S. M. Vaez Allaei, M. Sahimi, and M. R. Rahimi Tabar (unpublished).

[24] H. Hamzehpour and M. Sahimi, Phys. Rev. E **73**, 056121 (2006).
[25] See, for example, M. R. Rasaei and M. Sahimi, Transp. Porous Media (to be published).
[26] H. Hamzehpour, Ph. D. thesis, Institute for Advanced Studies in Basic Sciences, Zanjan, Iran, 2006 (unpublished).
[27] D. P. Landau and K. Binder, *A Guide to Monte Carlo Simulations in Statistical Physics*, 2nd ed. (Cambridge University Press, Cambridge, England, 2005); M. E. J. Newman and G. T. Barkema, *Monte Carlo Methods in Statistical Physics* (Oxford University Press, London, 1999).
[28] C. Deutsch and P. Cockerham, Math. Geol. **26**, 67 (1994).
[29] E. Aarts and J. Korst, *Simulated Annealing and Boltzmann Machines* (Wiley, New York, 1989).
[30] W. H. Press, B. P. Flannery, S. A. Teukolsky, and W. T. Vetterling, *Numerical Recipies*, 2nd ed. (Cambridge University Press, Cambridge, England, 1992).
[31] X. Cai and A. Odegard, in *Proceedings of the 2nd IEEE International Conference on Cluster Computing Germany*, (IEEE, New York, 2000), p. 185; T. Bohlen, Comput. Geosci. **28**, 887 (2002).
[32] S. Phadke, D. Bhardwaj, and S. Yerneni, in *Proceedings of the Conference and Exposition on Petroleum Geophysics*, Society of Petroleum Geologists (SPG, Houston, 2000), p. 168; N. L. Armstrong-Crews, in *Proceedings of the International Conference on Parallel and Distributed Processing Techniques and Applications (PDPTA)*), p. 1946 (unpublished).
[33] R. Sanchez, T. T. Tsotsis, and M. Sahimi, Chem. Eng. Sci. (to be published).